This article has been accepted for publication in a future issue of this journal, but has not been fully edited. Content may change prior to final publication. Citation information: DOI 10.1109/TPEL.2016.2632717, IEEE Transactions on Power Electronics



# Reduced Active Switch Front End Multi-Pulse Rectifier with Medium Frequency Transformer Isolation

José Juan Sandoval, *Student Member, IEEE*, Harish S. Krishnamoorthy, *Member, IEEE*, Prasad N. Enjeti, *Fellow, IEEE*, and Sewan Choi, *Senior Member, IEEE*

***Abstract*— This paper presents a reduced switch count multi-pulse rectifier with medium frequency (MF) transformer isolation. The proposed topology consists of a 3-phase push-pull based AC to DC rectifier with a MF AC link employing two active switches. A 3-phase, 5-limb, multi-winding MF transformer is employed for isolation. The secondary side of the transformer is connected in zig-zag configuration and is fed to two 6-pulse diode rectifiers, achieving 12-pulse rectifier operation. The primary advantage of the proposed system is reduction in size/weight/volume compared to the conventional 60 Hz magnetic transformer isolation rectifier system. Operating the transformer at 600 Hz is shown to result in three times reduction in size. Furthermore, the proposed system employs only two active semiconductor switching devices operating under a simple pulse width modulation scheme. Also the zig-zag transformer connection helps to balance leakage inductance on the secondary side. Detailed analysis, simulation, and experimental results on a 208$V_{l\text{-}l}$, 3.15 kW laboratory prototype are presented to validate the performance of the proposed approach.**

***Index Terms*—medium frequency isolation, multi-pulse rectifier, power density, three-phase AC-DC power conversion**

## I. Introduction

Multi-pulse rectifier systems are used in a wide variety of applications in the industry [1, 2]. Both isolated and non-isolated transformer configured multi-pulse rectifier systems have been in use [3-6]. The primary advantage of multi-pulse rectifier systems is high quality dc-output voltage with simultaneous elimination of low frequency harmonic currents at the input utility terminals. In particular, 12-pulse and 18-pulse rectifier systems result in input current THD less than 16%, thereby facilitating compliance with IEEE 519 harmonic current limits [7]. Nevertheless, much of these systems employ low frequency (50/60 Hz) magnetics that contribute to large size/weight/volume particularly in high power applications.

Reduction in size and weight is achieved with the half-power transformer based 12-pulse rectifier system as explained in [6]. In this approach, a line frequency transformer processing half the power is employed and thus size remains a concern. Furthermore, this system is not suitable in applications requiring to step down or step up the voltage level [6]. References [7-10] detail auto-transformer based multi-pulse rectifier systems. Reduction in size and weight is achieved due to reduced kVA rating of the auto-transformer configuration. References [7] and [8] report auto-transformer rectifier configurations with $0.18P_o$ and $0.38P_o$ ratings respectively compared to the $1.03P_o$ rating of the conventional 12-pulse multi-winding transformer. However, these auto-transformer configurations do not have galvanic isolation and employ 60 Hz magnetics. Thus, the use of line frequency magnetics continues to have a negative impact on the size/weight of the rectifier system.

References [11-14] detail modular three-phase power factor correction (PFC) AC to DC rectifier systems with high frequency magnetics. Despite the improvement in input current quality, these systems employ multiple power conversions and employ a high number of semiconductor devices. Furthermore, active PFC schemes require a significant sensing effort and are complicated to control. Also, EMI is a concern in these topologies due to their high switching frequency operation.

In contrast, the proposed topology shown in Fig. 1 seeks to improve over the existing 12-pulse AC to DC rectifier systems (isolated and auto-connected) by reducing size/weight/volume and improving the performance. The advantages of the proposed system architecture are:

1.) The approach employs medium frequency (600Hz) magnetics that is shown to improve power density by reducing the size/weight of the system [15, 16].
2.) The approach employs only two active semiconductor devices. This contributes to system simplicity and reduced cost.
3.) The $5^{th}$ and $7^{th}$ harmonics are eliminated in the input line current over a wide range of output voltage control thereby resulting in reduction in input current THD.
4.) Output voltage can be controlled by varying the duty cycle of the pulse width modulated signal.
5.) The system offers galvanic isolation between the input and output thereby minimizing the interference and contributing to safety.
6.) The approach is suitable for applications where power

José Juan Sandoval, Harish S. Krishnamoorthy, and Prasad N. Enjeti are with the Department of Electrical & Computer Engineering, Texas A&M University, College Station, TX 77843 USA (e-mail: jjsandoval@tamu.edu; h.s.k@ieee.org; enjeti@tamu.edu).

Sewan Choi is with the Department of Electrical and Information Engineering, Seoul National University of Science and Technology, Seoul 139-743, Korea. This work was supported in part by the National Research Foundation of Korea grant funded by Korea government (No. 2014R1A2A2A01003724) and in part by Overseas Research Professor Program of Seoul Tech. (e-mail: schoi@seoultech.ac.kr).

This article has been accepted for publication in a future issue of this journal, but has not been fully edited. Content may change prior to final publication. Citation information: DOI 10.1109/TPEL.2016.2632717, IEEE Transactions on Power Electronics



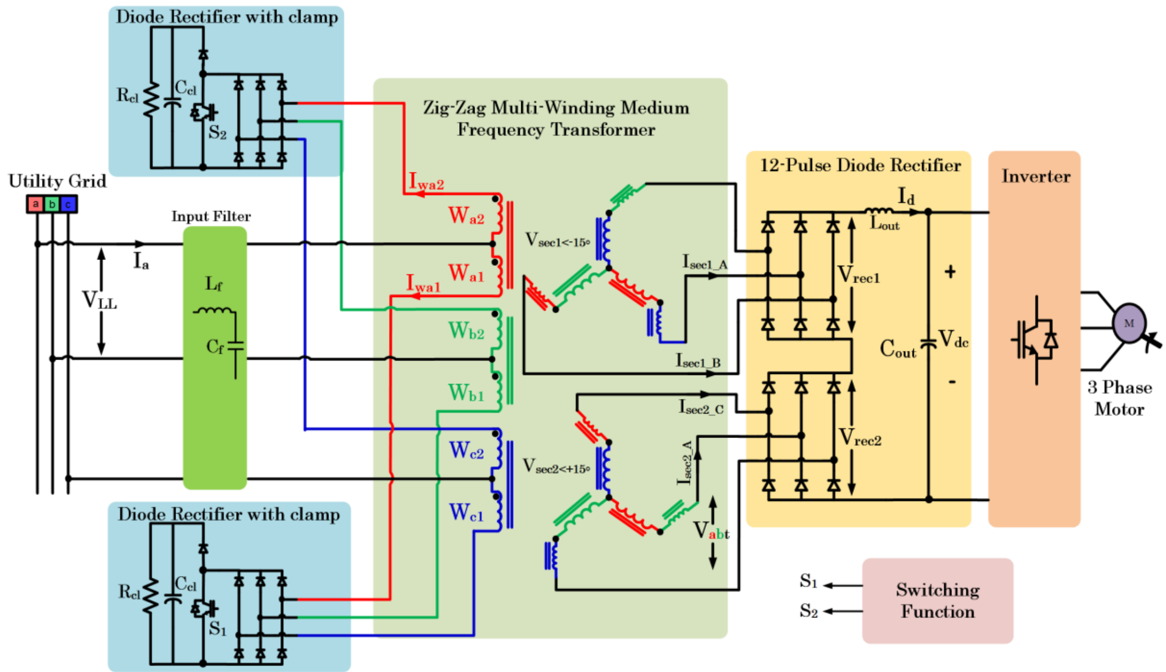


Fig. 1. Proposed 12-pulse AC-DC rectifier system with medium frequency transformer isolation employing two active switches. An example adjustable speed drive system is shown at the output.

density, performance and simplicity in control are of paramount importance.

7.) The secondary side of the MF transformer can be configured to higher-pulse operation (i.e. 18-pulse, 24-pulse) to further improve input current quality.

These benefits make the topology suitable for operation up to 480V three-phase systems for powering loads up to 150 kW. The paper details the analysis and design of the proposed multi-pulse rectifier system along with a design example. Simulation and experimental results are discussed on a scale-down laboratory prototype.

## II. Proposed Front-End Rectifier With Medium Frequency Transformer Isolation

The proposed system employing MF isolation with a multi-winding transformer is shown in Fig. 1. The operation of the proposed topology can be divided in the following stages: (A) diode rectifiers with clamp circuit, (B) MF multi-winding transformer, (C) 12-pulse diode rectifier, (D) modulation scheme, and (E) input current analysis.

### *A. Diode Rectifiers with Clamp Circuit*

This part of the system is composed of two 3-phase diode rectifiers, each connected to a high voltage active switch ($S_1$/$S_2$) and a clamp circuit, which consist of a capacitor and a bleeding resistor. The 3-phase AC link across the transformer windings is achieved by switching $S_1$ and $S_2$ complementarily with 50% duty cycle as first described in [18] and as shown in Fig. 2 (a), (b). The overall switching function for 50% duty cycle is shown in Fig. 2 (c). The primary windings of the zig-zag transformer can be divided into two sets that are 180° phase shifted in magnetic coupling, namely windings ($W_{a1}$, $W_{b1}$, $W_{c1}$) and windings ($W_{a2}$, $W_{b2}$, $W_{c2}$). As shown in Fig. 1, the center tap of each primary winding is connected to the utility grid. In addition, the switching terminals of windings ($W_{a1}$, $W_{b1}$, $W_{c1}$) are connected to a diode rectifier whose output is in turn connected to $S_1$. Similarly, the switching terminals of windings ($W_{a2}$, $W_{b2}$, $W_{c2}$) are connected to a diode rectifier whose output is in turn connected to $S_2$.

When $S_1$ is gated ON and $S_2$ is gated OFF, the switching terminals of windings ($W_{a1}$, $W_{b1}$, $W_{c1}$) are shorted through the diode rectifier while the switching terminals of windings ($W_{a2}$, $W_{b2}$, $W_{c2}$) are open. In essence, the switching terminals of windings ($W_{a1}$, $W_{b1}$, $W_{c1}$) are shorted to the utility's neutral point. Therefore, at this instant, the line-to-neutral voltages $V_{an}$, $V_{bn}$, and $V_{cn}$ appear across windings $W_{a1}$, $W_{b1}$, and $W_{c1}$ respectively. The voltages across windings ($W_{a2}$, $W_{b2}$, $W_{c2}$) have opposite polarity compared to the voltages across windings ($W_{a1}$, $W_{b1}$, $W_{c1}$) because they are 180° in magnetic coupling. Meanwhile, the induced voltages on the secondary side have the same polarity as the voltages across windings ($W_{a1}$, $W_{b1}$, $W_{c1}$).

When $S_1$ is gated OFF and $S_2$ is gated ON, the switching terminals of windings ($W_{a1}$, $W_{b1}$, $W_{c1}$) are open while the switching terminals of windings ($W_{a2}$, $W_{b2}$, $W_{c2}$) are shorted and are at the same potential as the utility's neutral point. At this instant, the line-to-neutral voltages $V_{an}$, $V_{bn}$, and $V_{cn}$ appear across windings $W_{a2}$, $W_{b2}$, and $W_{c2}$ respectively. The induced voltages on the secondary side and the voltages across windings ($W_{a1}$, $W_{b1}$, $W_{c1}$) have opposite polarity compared to the utility grid line-to-neutral voltages. The voltage polarity across each winding changes as $S_1$ and $S_2$ are switched. Therefore, by switching $S_1$ and $S_2$ at MF a 3-phase AC link is created.

The 3-phase AC link is simply a multiplication of the line-to-neutral voltages with a square wave switching function. Fig. 2(e) shows the mathematical AC voltage across winding $W_{a1}$ when the system operates at 50% duty cycle. With a line-to-neutral voltage as in (1) and a square wave switching function described by (2), the resulting voltage across the transformer winding $W_{a1}$ can be expressed as in (3). It is

This article has been accepted for publication in a future issue of this journal, but has not been fully edited. Content may change prior to final publication. Citation information: DOI 10.1109/TPEL.2016.2632717, IEEE Transactions on Power Electronics



evident that the frequency of the square wave switching function determines the fundamental frequency of the AC link created across the transformer windings. The voltages across windings $W_{b1}$ and $W_{c1}$ have a similar expression as in (3) but are 120° and 240° phase shifted respectively. The expression at (3) is valid for 50% duty cycle operation.

$$V_{an} = \sqrt{\frac{2}{3}} V_{LL} \sin(\omega_s t) \quad (1)$$

$$S_{sw} = \frac{4}{\pi} \sum_{n=1,3,5,...}^{\infty} \frac{1}{n} \sin(n\omega_{sqr} t) \quad (2)$$

$$V_{Wa1} = \sqrt{\frac{2}{3}} V_{LL} \sum_{n=1,3,5,...}^{\infty} \frac{2}{n\pi} \sin(\{n\omega_{sqr} \pm \omega_s\} \cdot t) \quad (3)$$

When the switching terminals of windings ($W_{a1}$, $W_{b1}$, $W_{c1}$) or ($W_{a2}$, $W_{b2}$, $W_{c2}$) are open, the clamp circuit provides a path for the energy stored in the leakage inductance of the windings. For example, when $S_1$ is OFF, the energy stored in the leakage inductance of windings ($W_{a1}$, $W_{b1}$, $W_{c1}$) is transferred to the capacitor which clamps to the highest line-to-line voltage. Furthermore, in order to avoid overlap (instances in which both $S_1$ and $S_2$ are ON) a dead time between $S_1$ and $S_2$ is necessary. During this dead time the clamp circuit also provides a path for the energy stored in the leakage inductance of the windings. The energy stored in the capacitor can be used to power a switch mode power supply (SMPS). This SMPS can power gate drive circuitry.

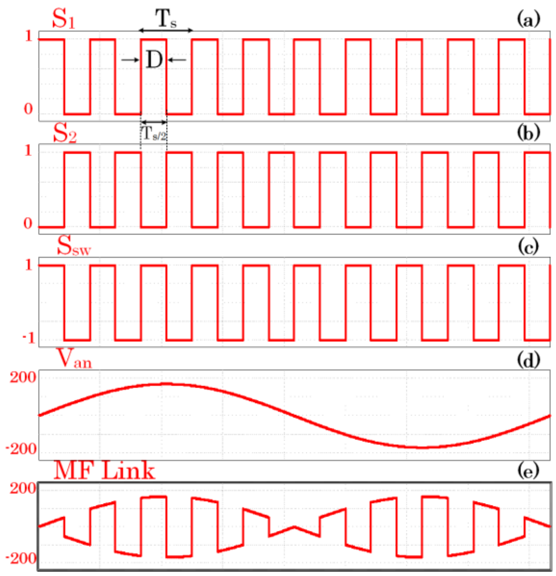


Fig. 2. (a) gating function for $S_1$; (b) gating function for $S_2$; (c) overall system switching function; (d) $V_{an}$, input line-to-neutral voltage; (e) Medium frequency AC link is the multiplication of $S_{sw}$ and $V_{an}$ created by switching $S_1$ and $S_2$ complementarily with 50% duty cycle.

## B. Medium Frequency Multi-Winding Transformer

The switching frequency of $S_1$ and $S_2$ determines the operating frequency of the transformer. The well-known trade-off between power density and efficiency must be considered when selecting the switching frequency. Operating at MF (600 Hz -1000 Hz) enables the transformer to be reduced in size and provides a good efficiency trade-off especially in high power applications [15]. Increasing the switching frequency to the kHz range increases transformer core loss and switching losses. Furthermore, operating in the kHz range increases the input EMI and introduces the need for additional EMI filtering at the input [8]. Thus, the transformer is designed to operate at 600 Hz.

Selection of the appropriate magnetic materials is also critical to achieve high power density. For high power MF applications, magnetic core materials such as ferrite, amorphous, and silicon steel should be considered [19]. Due to its high saturation flux density and relative low cost [20], a silicon steel core material was selected to build the MF transformer for the scaled down laboratory prototype. The transformer can be built using three 1-phase multi-winding transformers, or it can be a single 3-phase multi-winding transformer. To achieve a more compact design, a single 5-limb transformer is employed for isolation. The primary and secondary windings are wound around the interior three limbs of the transformer as depicted in Fig. 3. The exterior limbs can carry any unbalanced flux in the transformer avoiding core saturation [21].

Generally, in 12-pulse applications a star-delta winding connection is used in the secondary side to generate a net 30° phase difference. However, the leakage inductances of the terminals feeding the diode bridge rectifiers are not equal because the turns-ratio is different in the star-delta connected windings. This issue leads to unequal current sharing between the diode bridges [7]. To mitigate this problem, the secondary side of the MF transformer in the proposed system is connected in zig-zag. With zig-zag arrangement the leakage inductances on the secondary side are balanced because the turns-ratio of the windings per phase is the same.

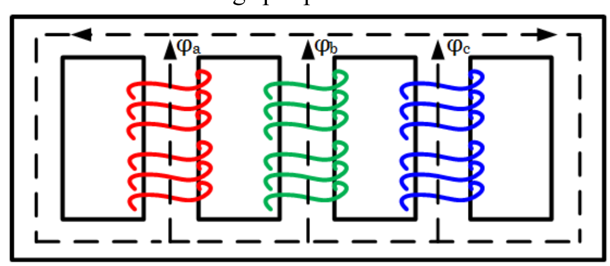


Fig. 3: Multi-winding 3-phase, 5-limb transformer.

The secondary windings are connected such that two sets of 3-phase voltages with a net 30° phase difference are fed to the 12-pulse diode rectifier. One set of 3-phase voltages is displaced by +15° with respect to the primary windings, while the second set of 3-phase voltages is displaced by -15° with respect to the primary windings. A phasor diagram of the primary side and secondary side voltages is shown in Fig. 4. To accomplish a net 30° phase difference, the windings turn-ratio must be set as defined by (4) and connected as shown in Fig. 5.

$$N_{P1} : N_{P2} : N_{S1} : N_{S2} : N_{S3} : N_{S4} = 1:1:\frac{\sqrt{3}-1}{\sqrt{6}}:\sqrt{\frac{2}{3}}:\frac{\sqrt{3}-1}{\sqrt{6}}:\sqrt{\frac{2}{3}} \quad (4)$$

The transformer's turn-ratio can be obtained by performing phasor operations. As shown in Fig. 4, the secondary side output voltage $V_{at}$ is desired to have a unity magnitude with a phase shift of +15° with respect to the primary line-to-neutral voltage $V_{an}$. Such a phasor can be obtained by adding a portion of phasor $V_{an}$ and a negative portion of phasor $V_{bn}$. The magnitudes of the phasor $V_{an}$ and $V_{bn}$ correspond to the turn-

This article has been accepted for publication in a future issue of this journal, but has not been fully edited. Content may change prior to final publication. Citation information: DOI 10.1109/TPEL.2016.2632717, IEEE Transactions on Power Electronics



ratio of the windings and can be found by solving (5). Breaking (5) into its real and imaginary components yields a system of two equations and two unknowns and therefore the magnitudes of $V_{an}$ and $V_{bn}$ can be obtained. Similar phasor operations can be performed to obtain the magnitudes of the phasors giving a secondary side output voltage $V_{as}$ with unity magnitude and a phase shift of -15° with respect to the primary line-to-neutral voltage. This zig-zag connection yields two set of voltages ($V_{abs}$, $V_{bcs}$, $V_{cas}$) and ($V_{abt}$, $V_{bct}$, $V_{cat}$) which have a 30° phase shift with respect to each other.

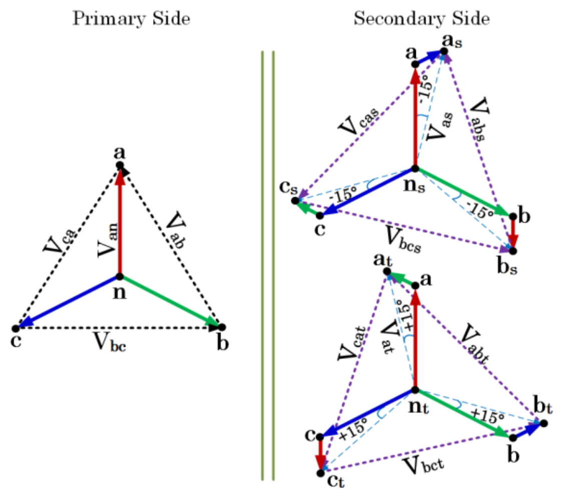


Fig. 4. Phasor diagram to obtain two sets of 3-phase voltages in the secondary side with a net 30° phase shift.

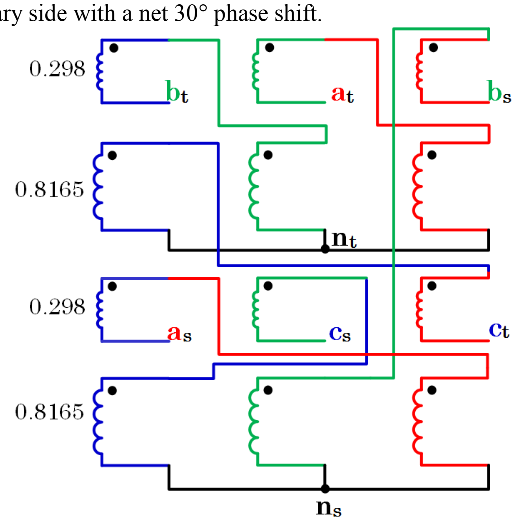


Fig. 5. Zig-zag connection of secondary windings. Interior limbs of 3-phase transformer, each limb has four secondary windings.

$$V_{an}\angle 0° + V_{bn}\angle -120° = 1\angle 15° \tag{5}$$

The VA rating of the multi-winding MF transformer can be calculated using the rms voltage and rms current of each winding under the assumption that the output current $I_d$ has negligible ripple. The relation between the line-to-line rms input voltage $V_{LL}$ and the output DC voltage is expressed as

$$V_{LL} = \frac{V_{dc}}{1.35 \cdot 2} \tag{6}$$

The rms value of the current through the primary windings is

$$I_{wa1} = 1.11 \cdot I_d \tag{7}$$

The rms value of the current through the secondary windings is

$$I_{as} = \sqrt{\frac{2}{3}} \cdot I_d = 0.816 I_d \tag{8}$$

The rms value of the voltage across the primary windings is

$$V_{wa1} = \frac{V_{LL}}{\sqrt{3}} = 0.577 V_{LL} = 0.214 V_{dc} \tag{9}$$

The rms voltage across the windings with turns ratio $N_{S1}$ is

$$V_{s1} = \frac{\sqrt{3}-1}{\sqrt{6}} \cdot \frac{V_{LL}}{\sqrt{3}} = 0.17 V_{LL} = 0.064 V_{dc} \tag{10}$$

Similarly, the rms voltage across the windings with turns ratio $N_{S2}$ is

$$V_{s2} = \sqrt{\frac{2}{3}} \cdot \frac{V_{LL}}{\sqrt{3}} = 0.47 V_{LL} = 0.175 V_{dc} \tag{11}$$

Then the sum total of the volt-ampere product of the MF transformer is (12)

$$VA_{tot} = 6 \cdot I_{wa1} \cdot V_{wa1} + 6 \cdot I_{as}(V_{s1} + V_{s2}) = 6.96 V_{LL} I_d = 2.58 V_{dc} I_d$$

Thus, the equivalent VA rating of the MF transformer is

$$VA_{eq} = \frac{1}{2} VA_{tot} = 1.29 V_{dc} I_d = 1.29 P_o \tag{13}$$

Although the VA rating of the proposed transformer configuration is slightly higher than the conventional 12-pulse isolation transformer ($1.03P_o$), the proposed transformer configuration does not carry the line frequency component. Instead, the transformer operates at MF enabling a size reduction.

### C. 12-Pulse Diode Rectifier

Two sets of 3-phase voltages with a net 30° phase difference are created with the zig-zag arrangement. Each set is fed to a 6-pulse diode rectifier achieving 12-pulse rectification. The operation of the bridge rectifiers is similar to the conventional line frequency 12-pulse configuration. The main difference is that the diodes should be able to switch at the operating frequency. The DC link output voltage $V_{dc}$ of the 12-pulse diode rectifier is calculated by (6). The design of the output inductor, $L_{out}$, and the output capacitor, $C_{out}$, is similar to the conventional line frequency diode rectifier and depend primarily on the requirements of the load.

### D. Modulation Scheme

A major advantage of the proposed system is that no closed loop control is required because the topology intends to replicate the performance of a conventional line frequency transformer. Therefore, no sensing is required in the proposed scheme. If output voltage regulation is desired, the proposed system can operate with simple variable duty cycle operation. This would require sensing the output DC voltage. Operation at 50% duty cycle provides the maximum MF AC link rms voltage. At duty cycles less than 50%, zero states are introduced in the MF AC link decreasing the overall output DC voltage. If the duty cycle is increased beyond 50%, short circuits occur across the transformer windings. Consequently, the modulation becomes simple and robust in contrast to other systems which employ complicated modulation strategies.

### E. Input Current Analysis

By virtue of the net 30° phase shift created by the zig-zag arrangement in the secondary side, the 5th, 7th, 17th, 19th, etc, harmonics are eliminated in the utility line currents. Mathematical analysis is provided for the line current in phase "a" through Fourier series and under the assumption of negligible ripple in the output DC current $I_d$. Ideally the input current $I_a$ divides equally through the center tap windings $W_{a1}$ and $W_{a2}$ and can be expressed as

$$I_a = I_{wa1} + I_{wa2} \tag{14}$$

The turns-ratio of the center-tap windings, $N_{P1}$ and $N_{P2}$, are the same. Thus, by VA balance the input current is expressed as

$$N_{P1}(I_{wa1} + I_{wa2}) = N_{P1} \cdot I_a = N_{S1}I_{as1} + N_{S2}I_{as2} + N_{S3}I_{as3} + N_{S4}I_{as4} \tag{15}$$

where $N_{S1}$, $N_{S2}$, $N_{S3}$, $N_{S4}$ are the turns ratio of the secondary windings associated with phase "a" and are determined by (4) and (5). Similarly, $I_{as1}$, $I_{as2}$, $I_{as3}$, and $I_{as4}$ are the currents flowing through the secondary windings associated with phase "a"; these currents can be expressed in terms of the currents flowing through the output 6-pulse diode rectifiers as follows:

$$I_{as1} = -I_{\mathrm{sec1\_}B} \tag{16}$$

$$I_{as2} = I_{\mathrm{sec1\_}A} \tag{17}$$

$$I_{as3} = -I_{\mathrm{sec2\_}C} \tag{18}$$

$$I_{as4} = I_{\mathrm{sec2\_}A} \tag{19}$$

Similarly, the currents flowing through the output 6-pulse diode rectifiers can be expressed as:

$$I_{\mathrm{sec1\_}A} = S_1\left(\omega t - \frac{\pi}{12}\right) \cdot S_{sw} \tag{20}$$

$$I_{\mathrm{sec1\_}B} = S_1\left(\omega t - \frac{\pi}{12} - \frac{2\pi}{3}\right) \cdot S_{sw} \tag{21}$$

$$I_{\mathrm{sec2\_}A} = S_1\left(\omega t + \frac{\pi}{12}\right) \cdot S_{sw} \tag{22}$$

$$I_{\mathrm{sec2\_}C} = S_1\left(\omega t + \frac{\pi}{12} + \frac{2\pi}{3}\right) \cdot S_{sw} \tag{23}$$

The -15° and +15° phase shift is evident from (20) and (22) respectively. $S_{sw}$ corresponds to the switching function described by (2) and $S_1(\omega t)$ corresponds to the quasi-square wave nature of the current in 6-pulse rectifiers and is expressed as:

$$S_1(\omega t) = \sum_{n=1,3,5,7}^{\infty} \left(\frac{4I_d}{n\pi} \cos\left(\frac{n\pi}{6}\right)\right) \cdot \sin(n\omega t) \tag{24}$$

Thus, the input current $I_a$ is determined by (25). The switching function, $S_{sw}$, is a square wave with duty cycle 0.5. Thus, squaring this function yields a constant one. After simplification $I_a$ is described by (26). From (26) it is observed that harmonics 5th, 7th, 17th, and 19th are eliminated as in conventional 12-pulse operation. This analysis demonstrates that the proposed front-end rectifier system with MF isolation can be a retrofit replacement of bulky line frequency transformers in conventional 12-pulse systems. The input current performance is maintained while improving power density with a reduced active switch count and simple modulation scheme. The theoretical THD value of the input current (16%) is the same as in the conventional 12-pulse rectifier. To improve the current performance, an input passive filter must be included as shown in Fig. 1. Since the line input current in the proposed system has identical harmonic spectrum as the line current in the conventional 12-pulse rectifier, the requirements of the passive filter in terms of size remain the same.

## III. Simulation Results

A 208 $V_{LL}$, 10 kW design example is considered to demonstrate the operation of the proposed front-end rectifier system in Fig. 1. The parameters in Table I were used for simulation in PSIM. The simulations were performed without an input passive filter to compare with a conventional 12-pulse rectifier. Adding a passive filter with $L_f$ = 1.7 mH (0.13 p.u) and $C_f$ = 140 µF results in a line current with THD <5 % and a system power factor >0.98.

TABLE I
Operating Conditions for the System in Fig. 1

| | |
|---|---|
| Grid voltage (line-to-line rms) | 208 V |
| Grid frequency | 50 Hz |
| Rectifier output voltage | 560 $V_{dc}$ |
| Rated power | 10 kW |
| Switching frequency ($f_{sqr}$) | 600 Hz |
| Output Inductor ($L_{out}$) | 2 mH |
| Output Capacitor ($C_{out}$) | 200 µF |

As stated in section II, a 3-phase MF AC link is created across the transformer windings by switching $S_1$ and $S_2$ complementarily. The 3-phase MF AC link can be observed in Fig. 6(a), it is evident that the voltages across the windings ($W_{a1}$, $W_{b1}$, $W_{c1}$) are displaced by 120° from each other. The voltages across the windings ($W_{a2}$, $W_{b1}$, $W_{c2}$) are also a set of 3-phase voltages with 120° phase shift; however they are opposite in polarity with respect to the voltages across the first set of windings. Fig. 6(b) shows the line-to-line voltages ($V_{abs}$, $V_{abt}$) which feed the 12-pulse diode rectifier. The voltages are 30° phase shifted with respect to each other as in conventional 12-pulse operation. The input currents of the diode rectifiers $I_{\mathrm{sec1\_A}}$ and $I_{\mathrm{sec2\_A}}$ in Fig. 6(c) also demonstrate the 30° phase shift. The FFT of the voltage across winding $W_{a1}$ confirms MF operation as shown in Fig. 7. The fundamental voltage frequency occurs at 600±50 Hz; this enables the use of MF transformers thereby reducing the weight/size of the system [15]. The output DC voltage and the individual rectified

$$I_a = \left[\sqrt{\frac{2}{3}}\left\{S_1\left(\omega t - \frac{\pi}{12}\right) + S_1\left(\omega t + \frac{\pi}{12}\right)\right\} - \frac{-1+\sqrt{3}}{\sqrt{6}}\left\{S_1\left(\omega t - \frac{\pi}{12} - \frac{2\pi}{3}\right) + S_1\left(\omega t + \frac{\pi}{12} + \frac{2\pi}{3}\right)\right\}\right] \cdot S_{sw}^2 \tag{25}$$

$$I_a = \frac{4\sqrt{3} \cdot I_d}{\pi}\left[\sin(\omega_s t) - \frac{1}{11}\sin(11 \cdot \omega_s t) - \frac{1}{13}\sin(13 \cdot \omega_s t) + \frac{1}{23}\sin(23 \cdot \omega_s t) + \frac{1}{25}\sin(25 \cdot \omega_s t) + \ldots\right] \tag{26}$$

This article has been accepted for publication in a future issue of this journal, but has not been fully edited. Content may change prior to final publication. Citation information: DOI 10.1109/TPEL.2016.2632717, IEEE Transactions on Power Electronics



voltages $V_{rec1}$ and $V_{rec2}$ are depicted in Fig. 8. The 30° phase shift is also noticeable in the individual rectified voltages ensuring 12-pulse operation.

Fig. 9(a) shows the input current for phase "a"; 12-pulse operation can be observed in the input current. The simulated THD is 16%. The FFT of the line current is shown in Fig. 9(b); the dominant harmonics are $11^{th}$ and $13^{th}$ as in conventional 12-pulse configuration. This is in agreement with the input current analysis and demonstrates that the proposed topology can be a retrofit replacement of the bulky line frequency multi-winding transformer in conventional 12-pulse systems.

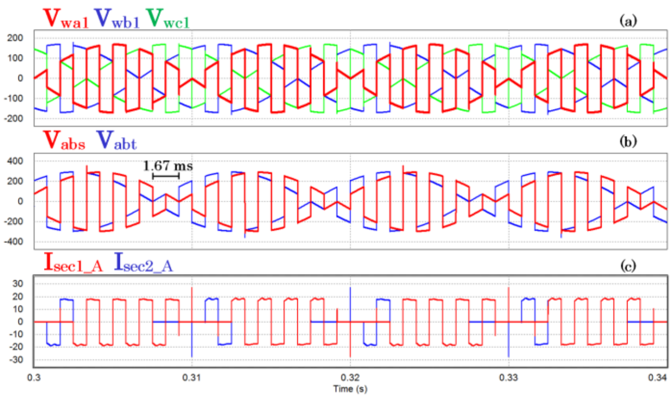


Fig. 6. (a) Transformer winding voltage due to 50% duty cycle operation of $S_1$ and $S_2$ at 600 Hz. Note the voltages across windings $W_{a1}$, $W_{b1}$, $W_{c1}$ are displaced by 120°; (b) Line-to-line voltages $V_{abs}$ and $V_{abt}$ are 30° phase shifted. (c) Rectifier input currents on the secondary side of the transformer.

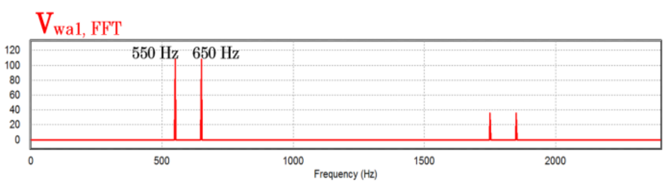


Fig. 7. FFT of the voltage across transformer winding $W_{a1}$. Fundamental frequency of operation is 600±50 Hz enabling the use of MF transformers. Other components appear at $3f_s$ ±50 Hz.

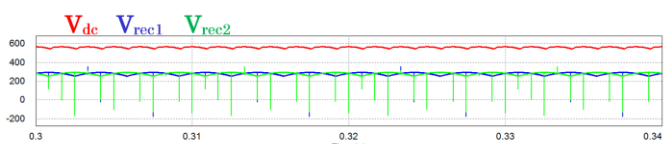


Fig. 8. DC output voltage at 560V. Individual rectified voltages have 30° phase shift as in conventional 12-pulse operation.

In addition to the simulations in PSIM, the magnetic behavior of the proposed MF transformer was simulated using Ansys Maxwell finite element analysis (FEA) software. The primary windings of the modelled transformer were excited using the voltage expression derived in (3). The material of the core was selected to be M19 silicon steel which has a saturation flux density of 1.4 T at MF. A plot of the magnetic field density for a 2D simulation of the proposed transformer is given in Fig. 10. From the simulation, it is shown that the flux density is higher in the interior three-limbs of the transformer as expected. The core of the transformer is shown to operate at 0.8 T which is below the saturation region. In Fig. 11, the corresponding magnetic flux lines plot is presented. The flux lines also concentrate along the interior three-limbs of the transformer. Using the M19 core loss data at 600 Hz, the FEA software is used to simulate the core losses of the MF transformer. The simulated core losses shown in Fig. 12 are compared with the actual losses to evaluate the efficiency of the proposed topology as discussed in the next section.

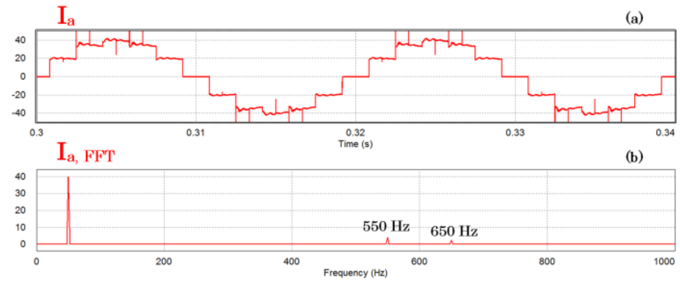


Fig. 9. (a) Input line current for phase "a"; 12-pulse operation is evident, (b) FFT of the input current verifies 12-pulse operation. Note: the dominant harmonics are $11^{th}$ and $13^{th}$ (550 Hz and 650 Hz). Simulated current THD is 16%.

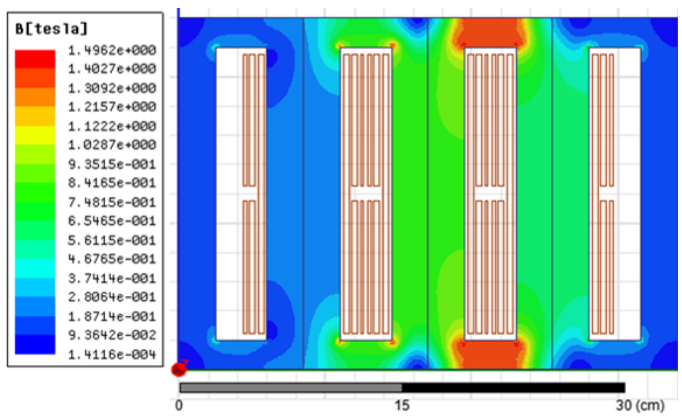


Fig. 10. Magnetic field density plot of the proposed 5-limb, 3-phase transformer when excited with a MF AC link. The 2D dimensions of the transformer are (34 cm X 24 cm). The model has a depth of 5cm.

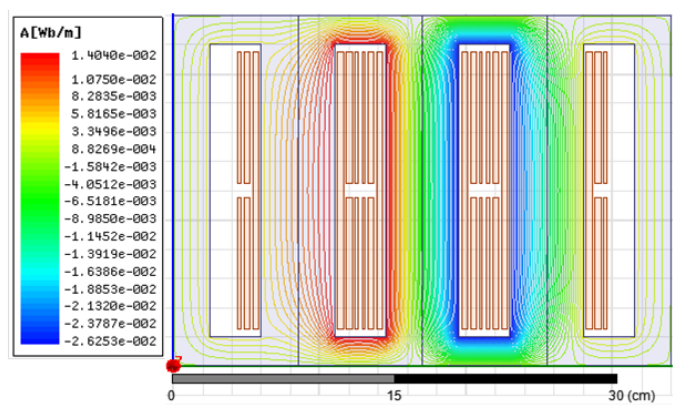


Fig. 11. Magnetic flux lines of the proposed 5-limb, 3-phase transformer when excited with a MF AC link. The flux lines concentrate in the interior three limbs of the transformer.

## IV. Efficiency Analysis of Multi-Pulse AC-DC Conversion Stage

The efficiency of the proposed reduced active switch multi-pulse rectifier can be calculated by analyzing switching and conduction losses, and transformer core and winding losses. The switching/conducting characteristics of the semiconductor

This article has been accepted for publication in a future issue of this journal, but has not been fully edited. Content may change prior to final publication. Citation information: DOI 10.1109/TPEL.2016.2632717, IEEE Transactions on Power Electronics



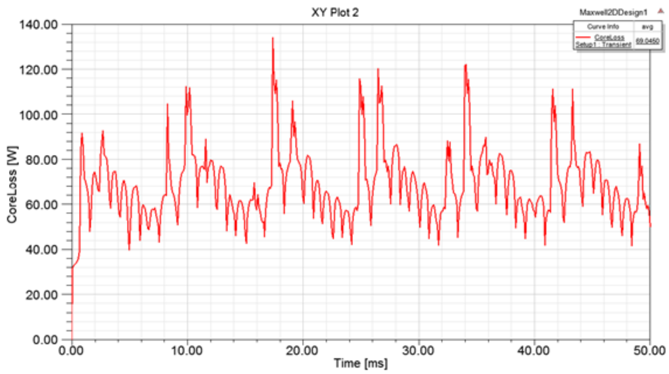


Fig. 12. Simulated core losses using FEA software. The average core loss is 69 W.

devices in Table II were used for power loss analysis. The currents and voltages through the semiconductor devices are obtained from the simulation results in Section III. From calculation, it is determined that the switching and conduction losses of the active switches ($S_1/S_2$) account for 18% of the total losses. Similarly, the diode clamp circuit accounts for 42% of the system's losses while the 12-pulse diode rectifier on the secondary side accounts for 15% of the losses.

TABLE II
SEMICONDUCTOR DEVICES USED FOR POWER LOSS ANALYSIS

| System Component | Part Number | Manufacturer |
|---|---|---|
| $S_1/S_2$ | IRG4PH50SPbF | Infineon |
| Diode clamp circuit | C4D40120D | Cree |
| 12-pulse diode rectifier | C3D20060D | Cree |

An estimate of the transformer core losses was obtained using FEA analysis. The FEA simulation yields an average core loss of 69 W when the transformer primary windings are excited with a 3-phase MF AC link. The FEA simulation results were experimentally verified through an open circuit test of the MF transformer. Through experiments, a core loss of 80 W was obtained. The difference between the simulated and tested core losses occurs because the FEA model cannot account for all physical effects in a core with laminations [22]. The total transformer losses account for 25% of the system's losses. Using finer grades of steel or amorphous materials would decrease the transformer losses but the increase in cost must be considered [15]. The breakdown of the system losses is shown in Fig. 13. Overall, the efficiency of the proposed system is calculated to be 96.5%.

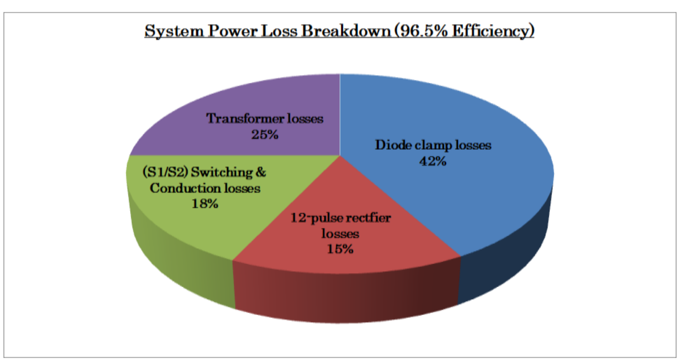


Fig. 13. System power loss breakdown for a 10 kW design example. The efficiency of the system is 96.5%.

## V. COMPARATIVE EVALUATION OF THE PROPOSED MULTI-PULSE RECTIFIER

In this section, the proposed multi-pulse front-end rectifier is compared with other existing schemes. The multi-pulse schemes considered for evaluation include the conventional 12-pulse rectifier, the half power 12-pulse rectifier, and two active techniques. The results of the comparison are shown in Table III. The proposed scheme uses only two active switches reducing the gate drive circuitry allowing for a compact system but the active switches must be rated for $2V_{LL}$. Due to the low number of active switches and simple modulation scheme, the proposed scheme has a low realization complexity compared to the three-phase modular PFC scheme. Similar to the active 12-pulse scheme, the sensing effort and modulation complexity of the proposed scheme is low which is attractive in industrial settings.

Among the five compared topologies, only in the proposed topology the phase-shifting transformer ($1.29P_o$) operates at MF with galvanic isolation. Operating at MF enables the power density (W/L) of the proposed phase-shifting transformer to be the highest among the topologies employing phase-shifting transformers. Power density is defined in (27). For power density calculation, the power rating and physical size of the transformers/matching inductors reported in [8] were used. The proposed zig-zag MF isolation transformer rated at 4 kW has a 980 W/L power density, which is nearly 3.4 times larger than the power density of the conventional line frequency 12-pulse isolation transformer.

Compared to the half power 12-pulse scheme described in [6], the power density of the proposed transformer configuration is nearly 3.9 times larger. Similarly, compared to the active 12-pulse scheme in [8] the power density of the proposed transformer configuration is about 2.8 times larger. This advantage in power density makes the proposed topology very attractive in applications where size is a constraint and isolation is required.

$$PowerDensity = \frac{OutputPower(W)}{Volume(L)} \qquad (27)$$

In addition, the volume of the proposed MF transformer is compared to the volume of a line frequency transformer through Ansys Maxwell FEA modeling. Two 3-phase transformers, one operating at line frequency and the other at MF frequency, were modeled for the same output load (4 kW), input voltage (208 $V_{l\text{-}l}$) and efficiency (~98%) requirements. Also, the same M19 silicon steel core material was considered for comparison. Considering the B-H curves of the M19 material at different operating frequencies, a peak flux density of 1.6 T with 105 primary turns was used for the line frequency transformer design while a peak flux density of 0.8T with 68 primary turns was used for the MF transformer design. A comparison of the size between the 3-phase line-frequency transformer and the 3-phase MF transformer is shown in Fig. 14. For the same output load, input voltage, and transformer efficiency requirements the line frequency transformer has a volume of 13.8 L (51 cm x 36 cm x 7.5 cm) while the MF transformer has a volume of 4 L (34 cm x 24 cm x 5 cm). Thus, the volume of the MF transformer is 30% of the volume of the line frequency transformer.

This article has been accepted for publication in a future issue of this journal, but has not been fully edited. Content may change prior to final publication. Citation information: DOI 10.1109/TPEL.2016.2632717, IEEE Transactions on Power Electronics



TABLE III
COMPARATIVE EVALUATION OF PROPOSED RECTIFIER WITH OTHER SCHEMES

| Topologies | | Conventional 12-Pulse | Half Power 12-Pulse | Active 12-Pulse [8] | Three single-phase PFC | Proposed |
|---|---|---|---|---|---|---|
| Configuration | | ac-dc | ac-dc | ac-dc-dc | ac-dc-dc | ac-ac-dc |
| No. of active switches | front-end | ------ | ------ | ------ | 3 | 2 |
| | dc-dc | ------ | ------ | 4 | 12 | ------ |
| | Total | ------ | ------ | 4 | 15 | 2 |
| Galvanic Isolation | | Yes | No | No | No | Yes |
| Sensing effort & modulation complexity | | None | Low | Low | High | Low |
| Phase-Shifting Transformer VA rating (operation frequency) | | $1.03P_o$ (line frequency) | $0.5P_o$ (line frequency) | $0.38P_o$ (line frequency) | ------ | $1.29P_o$ (medium frequency) |
| Power Density of Phase-Shifting transformer (Output-Watts/Liters) | | 290 | 252* | 352* | ------ | 980 |

*The volume for these topologies was obtained using the physical size of the phase-shifting transformer and the size of the matching inductors reported in [8]

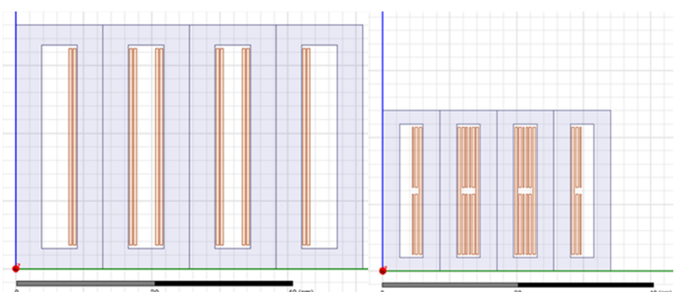

Fig. 14. Size comparison of 3-phase transformers. Line frequency transformer (left) has a volume of 13.8 L while the medium frequency transformer (right) has a volume of 4.1 L.

## VI. EXPERIMENTAL RESULTS

In order to validate the proposed topology a scaled-down laboratory prototype rated at 3.15 kW is built and tested. The input 3-phase line-to-line voltage is $208V_{rms}$ with fundamental frequency of 50 Hz. A small input passive filter with $L_f$=100 μH was used. The switching frequency of the active devices, namely $S_1$ and $S_2$, is set to 600 Hz. The clamp circuit is composed of a film capacitor $C_{cl}$=10 μF and $R_{cl}$=10 kΩ. The gate drive signals for the active switching devices are generated using a Texas Instruments microcontroller. Within the microcontroller, a dead time of 2μs is assigned to the gating signals of $S_1$ and $S_2$ to avoid overlap operation. The zig-zag MF transformer is designed to operate at the desired switching frequency and is built using silicon steel material. Fig. 15 shows the MF transformer used for the hardware experiments.

The experimental results are shown to be similar to simulation results. Fig. 16 shows the 3-phase MF AC link across windings $W_{a1}$, $W_{b1}$, and $W_{c1}$. It is evident that the set of 3 phase voltages are displaced by 120° (6.67 ms) from each other. Operation at MF is confirmed from Fig. 17. The FFT of the voltage $V_{wa1}$ shows fundamental components at 550 Hz and 650 Hz enabling the transformer to operate at MF. From Fig. 18, 12-pulse operation is observed; the secondary side voltages $V_{abs}$ and $V_{abt}$ show a net 30° phase shift (1.67 ms) with respect to each other. This figure also shows a smooth DC output voltage as in 12-pulse operation. The line input current $I_a$ is shown in Fig. 19 along with its FFT. The frequency spectrum shows that the $5^{th}$, $7^{th}$, $17^{th}$, $19^{th}$ harmonics have been eliminated confirming 12-pulse operation. The measured THD of the current is 17% but can be improved with an input passive filter with $L_f$ = 0.13 p.u. The measured $11^{th}$ and $13^{th}$ harmonic of the input current are about 10% and 7% respectively from the fundamental. From Fig. 20, high displacement power factor is shown between the line-to-neutral voltage $V_{an}$ and the line input current $I_a$. Furthermore, Fig. 20 shows that the effect of the switching frequency on the utility voltage is minimal.

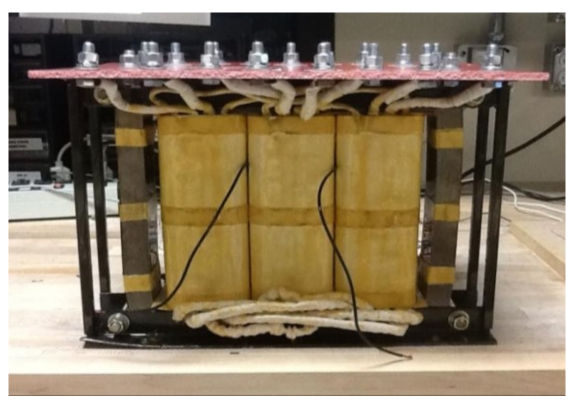

Fig. 15. Medium frequency 600 Hz transformer with silicon steel core (Volume = 4.08 L; Dimensions: 34 cm x 24 cm x 5 cm).

## VII. CONCLUSION

This paper proposes a reduced switch multi-pulse rectifier with MF transformer isolation employing two active semiconductor devices. It has been shown that operating at a MF of 600 Hz the transformer size is 1/3 of the equivalent 60 Hz design. A 10 kW design example has been shown to

This article has been accepted for publication in a future issue of this journal, but has not been fully edited. Content may change prior to final publication. Citation information: DOI 10.1109/TPEL.2016.2632717, IEEE Transactions on Power Electronics



achieve 96.5% efficiency. Simulation and experimental results on a laboratory prototype demonstrate the 12-pulse operation with high input current quality. Overall, the advantages of the system include high power density, reduced active switch count, and simple pulse width modulation scheme.


Fig. 16. Experimental results: Ch.1: Voltage across winding $W_{a1}$; Ch.2: Voltage across winding $W_{b1}$; Ch.3: Voltage across winding $W_{c1}$. Note: voltages are displaced by 120° with respect to each other.

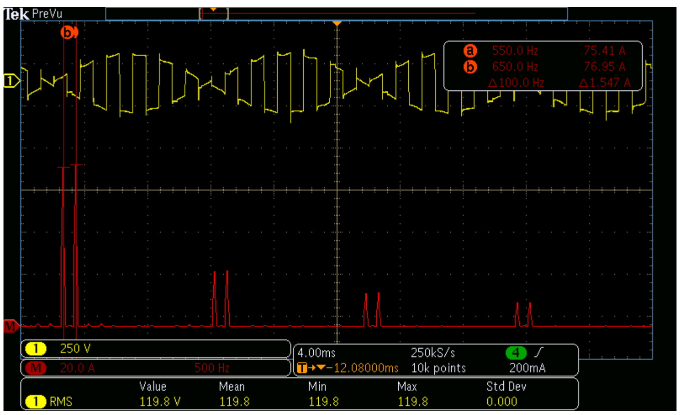


Fig. 17. Experimental results: Ch. 1: Primary side voltage $V_{wa1}$; Ch. M: FFT of $V_{wa1}$ shows fundamental components at 550 Hz and 650 Hz enabling MF operation.

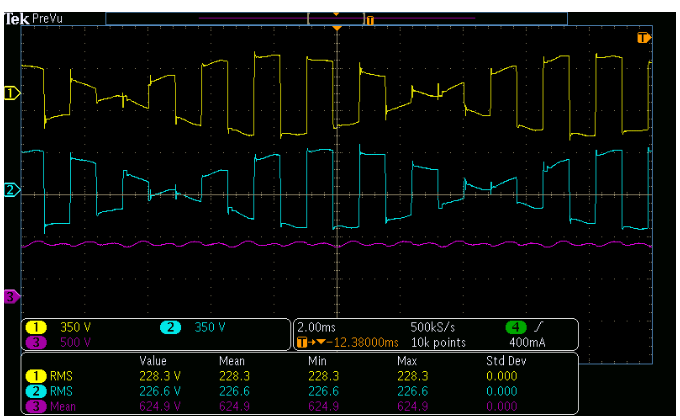


Fig. 18. Experimental results: Ch.1: Line-to-line voltage on the secondary side $V_{abs}$; Ch.2: Line-to-line voltage on the secondary side $V_{abt}$; Ch.3: DC output voltage. Note: $V_{abs}$ and $V_{abt}$ are displaced by 30° from each other to achieve 12-pulse rectification.

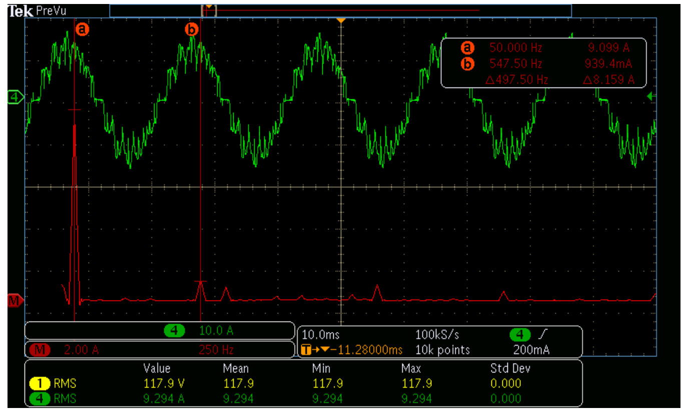


Fig. 19. Experimental results: Ch.4: Line input current $I_a$; Ch. M: FFT of $I_a$ shows dominant harmonics to be $11^{th}$ (550 Hz) and $13^{th}$ (650 Hz) as in 12-pulse operation. The $5^{th}$, $7^{th}$, $17^{th}$, and $19^{th}$ harmonics are eliminated. The measured THD is 17%.

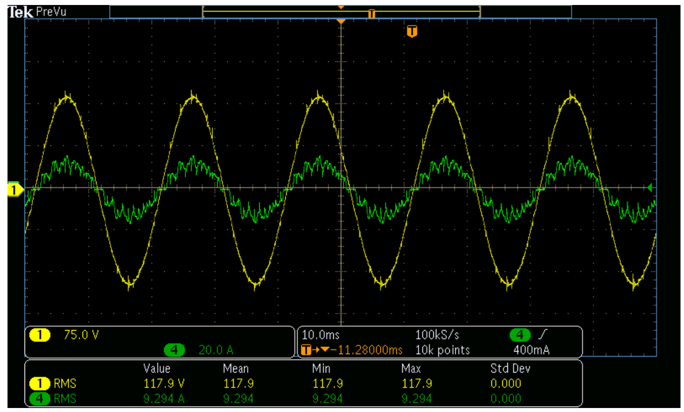


Fig. 20. Experimental results: Ch.1: Utility line-to-neutral voltage $V_{an}$; Ch.4: Line input current $I_a$.

## REFERENCES


[1] R. A. Hanna and S. Prabhu, "Medium-voltage adjustable speed drives-users' and manufacturer's experience," *IEEE Transactions on Industry Applications,* vol. 33, pp. 1407-1415, 1997.

[2] G. Song, M. Heldwein, U. Drofenik, J. Minibock, K. Mino, and J. W. Kolar, "Comparative Evaluation of Three-Phase High-Power-Factor AC-DC Converter Concepts for Application in Future More Electric Aircraft," *IEEE Transactions on Industrial Electronics,* vol. 52, pp. 727-73, June 2005.

[3] Toshiba. (April 20). *Toshiba MV Drives*. Available: http://www.toshiba.com/ind/data/tag_files/MTX_NEMA_3R_MV_Brochure_3002.pdf

[4] GE. (2015, April 20). *TM-GE MV Drives*. Available: http://www.wmea.net/Technical%20Papers/GE%20Medium%20Voltage%20Drives.pdf

[5] M. Swamy, T. Kume, and N. Takada, "A Hybrid 18-Pulse Rectification Scheme for Diode Front-End Rectifiers With Large DC Bus Capacitors," *IEEE Transactions on Industry Applications,* vol. 46, pp. 2484-2494, Nov-Dec. 2010.

[6] M. M. Swamy, "Uncontrolled and Controlled Rectifiers," in *Power Systems*, 3rd ed: CRC Press, 2012.

[7] S. Choi, P. N. Enjeti, and I. J. Pitel, "Polyphase transformer arrangements with reduced kVA capacities for harmonic current reduction in rectifier-type utility interface," *IEEE Transactions on Power Electronics,* vol. 11, pp. 680-690, September 1996.

[8] M. M. Swamy, "An Electronically Isolated 12-Pulse Autotransformer Rectification Scheme to Improve Input Power Factor and Lower Harmonic Distortion in Variable-Frequency Drives," *IEEE Transactions on Industry Applications,* vol. 51, pp. 3986-3994, Sept.-Oct. 2015.

[9] S. Choi, "A three-phase unity-power-factor diode rectifier with active input current shaping," *IEEE Transactions on Industrial Electronics,* vol. 52, pp. 1711-1714, Dec. 2005.

This article has been accepted for publication in a future issue of this journal, but has not been fully edited. Content may change prior to final publication. Citation information: DOI 10.1109/TPEL.2016.2632717, IEEE Transactions on Power Electronics



[10] G. R. Kamath, D. Benson, and R. Wood, "A Compact Autotransformer based 12-pulse rectifier circuit," in *The 27th Annual Conference of the IEEE Industrial Electronics Society, 2001. IECON*, Denver, CO, 2001, pp. 1344-1349.

[11] M. Swamy and A. Balakrishnan, "Three, single-phase power factor correction (PFC) boost converters for use with three-phase, 3-wire variable frequency drive systems," in *2015 IEEE Energy Conversion Congress and Exposition*, 2015, pp. 6993-7000.

[12] G. Spiazzi and F. C. Lee, "Implementation of single-phase boost power-factor-correction circuits in three-phase applications," *IEEE Transactions on Industrial Electronics,* vol. 44, pp. 365-371, 1997.

[13] Y. K. E. Ho, S. Y. R. Hui, and Y.-S. Lee, "Characterization of single-stage three-phase power-factor-correction circuits using modular single-phase PWM DC-to-DC converters," *IEEE Transactions on Power Electronics,* vol. 15, pp. 62-71, Jan 2000 2000.

[14] H. S. Kim, W. Baek, M. H. Ryu, J. H. Kim, and J. H. Jung, "The High-Efficiency Isolated AC-DC Converter Using the Three-Phase Interleaved LLC Resonant Converter Employing the Y-Connected Rectifier," *IEEE Transactions on Power Electronics,* vol. 29, pp. pp. 4017-4028, August 2014.

[15] M. Kang, P. N. Enjeti, and I. J. Pitel, "Analysis and design of electronic transformers for electric power distribution sytem," *IEEE Transactions on Power Electronics,* vol. 14, pp. 1133-1141, Nov. 1999.

[16] H. Krishnamoorthy, P. Garg, and P. Enjeti, "Simplified medium/high frequency transformer isolation approach for multi-pulse diode rectifier front-end adjustable speed drives," in *2015 IEEE Applied Power Electronics Conference and Exposition (APEC)*, 2015, pp. 527-534.

[17] ABB. (June 10). *ABB drives for marin Medium voltage drives for reliable and efficient operations at sea*. Available: https://library.e.abb.com/public/2e7b508ea530471ac125785b00446c95/Marine%20brochure%20RevB_lowres.pdf

[18] R. Gupta, K. K. Mohapatra, N. Mohan, G. Castelino, K. Basu, and N. Weise, "Soft switching power electronic transformer," United States Patent 8,446,743, May 21, 2013.

[19] W. M. Colonel and T. Mclyman, *Transformer and Inductor Design Handbook* vol. 3rd ed. Boca Raton, FL USA: CRC Press, 2004.

[20] X. She, A. Q. Huang, and R. Burgos, "Review of Solid-State Transformer Technologies and Their Application in Power Distribution Systems," *IEEE Journal of Emerging and Selected Topics in Power Electronics,* vol. 1, pp. 186-198, 2013.

[21] C.-k. Leung, D. S., S. Baek, and B. S., "Design considerations of high voltage and high frequency three phase transformer for Solid State Transformer application," in *2010 IEEE Energy Conversion Congress and Exposition (ECCE)*, 2010, pp. 1551-1558.

[22] ANSYSMaxwellTutorial. Example (2D/3D) Transient - Core loss.

**José Juan Sandoval** (S'11) received the B.S. degree in electrical engineering from Texas A&M University, College Station, TX, USA, in 2011. He is currently pursuing the Ph.D. degree in electrical engineering as a Gates Millennium Scholar at Texas A&M University, College Station, TX, USA.

He is also recipient of the Texas A&M Dissertation Fellowship and the Thomas Powell'62 Fellowship. His current research interests include high-power density three-phase ac-dc conversion, electric/hybrid vehicle battery chargers, and renewable energy grid integration.

**Harish S. Krishnamoorthy** (S' 12-M'15) received the B. Tech. degree in electrical and electronics engineering from the National Institute of Technology, Tiruchirappalli, India, in 2008 and the Ph.D. degree in electrical engineering at Texas A&M University, College Station, TX, USA, in 2015.

From 2008 to 2010, he was an Engineer in General Electric Energy, India. His current research interests include high power density converter design, renewable energy conversion, etc. He holds a U.S patent and several journal publications.

**Prasad N. Enjeti** (M'85–SM'88–F'00) received the B.E. degree from Osmania University, Hyderabad, India, in 1980, the M.Tech degree from Indian Institute of Technology, Kanpur, in 1982, and the Ph.D. degree from Concordia University, Montreal, Canada, in 1988, all in electrical engineering.

He has been a member of Texas A&M University Faculty since 1988. He is widely acknowledged to be a Distinguished Teacher, Scholar, and Researcher. He currently holds the TI-Professorship in analog engineering and serves as the Associate Dean for academic affairs with the College of Engineering. His research emphasis on industry-based issues, solved within an academic context, has attracted significant external funding. His primary research interests are in advancing power electronic converter designs to address complex power management issues, such as active harmonic filtering, adjustable speed motor drives, wind and solar energy systems, and designing high temperature power conversion systems with wide band-gap semiconductor devices. In 2004, he received a Distinguished Achievement Award for teaching from Texas A&M University. He is a recipient of the IEEE PELS R. David Middlebrook Technical Achievement Award from the IEEE Power Electronics Society in 2012.

**Sewan Choi** (S'92-M'96-SM'04) received the B.S. degree in electronic engineering from Inha University, Incheon, Korea, in 1985 and the M.S. and Ph.D. degrees in electrical engineering from Texas A&M University, College Station, TX, in 1992 and 1995, respectively. From 1985 to 1990, he was with Daewoo Heavy Industries as a Research Engineer. From 1996 to 1997, he was a Principal Research Engineer at Samsung Electro-Mechanics Co., Korea. In 1997, he joined the Department of Electrical and Information Engineering, Seoul National University of Science and Technology, Seoul, Korea. His research interests include power conversion technologies for renewable energy systems and energy storage systems and DC-DC converters and battery chargers for electric vehicles. He is an Associate Editor of the IEEE TRANSACTIONS ON POWER ELECTRONICS.